

# Selective area grown semiconductor-superconductor hybrids: a basis for topological networks

S. Vaitiekėnas,<sup>1</sup> A. M. Whiticar,<sup>1</sup> M. T. Deng,<sup>1</sup> F. Krizek,<sup>1</sup> J. E. Sestoft,<sup>1</sup>  
S. Marti-Sanchez,<sup>2</sup> J. Arbiol,<sup>2,3</sup> P. Krogstrup,<sup>1</sup> L. Casparis,<sup>1</sup> and C. M. Marcus<sup>1</sup>

<sup>1</sup>Center for Quantum Devices and Station Q Copenhagen,  
Niels Bohr Institute, University of Copenhagen, Copenhagen, Denmark

<sup>2</sup>Catalan Institute of Nanoscience and Nanotechnology (ICN2),  
CSIC and BIST, Campus UAB, Bellaterra, Barcelona, Catalonia, Spain

<sup>3</sup>ICREA, Pg. Lluís Companys 23, 08010 Barcelona, Catalonia, Spain

Majorana zero modes (MZMs) at the ends of one-dimensional topological superconductors are expected to exhibit non-Abelian braiding statistics [1, 2], providing naturally fault-tolerant qubits [3, 4]. Complex networks for braiding [5, 6], interference-based topological qubits [7–9] and topological quantum computing architectures [10] require either branched nanowires [11] or two-dimensional hybrid heterostructures [12] confined by etching and gating [13–15], each bringing challenges to scaling. Here, we demonstrate the viability of selective area grown (SAG) Al-InAs hybrid wires that can be patterned into structures with branches and loops, providing a new, flexible platform for topological superconducting networks. We find proximity-induced superconductivity with a hard induced gap and  $2e$ -periodic Coulomb blockade, indicating strongly suppressed quasiparticle poisoning. The observed overshoot of Coulomb blockade peak spacing in a parallel magnetic field is consistent with interacting MZMs, with an amplitude consistent with previous experiments [16]. We also measure electron phase-coherence length and spin-orbit coupling strength via interference measurements in an Aharonov-Bohm ring.

Following initial theoretical proposals [17, 18], a number of experiments have reported signatures of Majorana zero modes (MZMs) in hybrid semiconductor-superconductor nanowires [19], including zero-bias conductance peaks [14, 15, 20–26] and Coulomb blockade peak spacing oscillations [16, 27]. To date, experiments have used individual vapor-liquid-solid (VLS) nanowires [20–25] or gate-confined two-dimensional heterostructures [14, 15]. Within these approaches, constructing complex topological devices and networks containing branches and loops [5–10] is a challenge. Recently, branched and looped VLS growth has been developed toward this goal [11, 28].

In this Letter, we investigate a novel approach to the growth of semiconductor-superconductor hybrids that allows deterministic on-chip patterning of topological superconducting networks based on SAG. We characterize key physical properties required for building Majorana

networks, including a hard superconducting gap, induced in the semiconductor, phase-coherence length of several microns, strong spin-orbit coupling, and Coulomb blockade peak motion compatible with interacting Majoranas. Overall, these properties show great promise for SAG-based topological networks.

Selective area growth was realized on an InP substrate with a pre-patterned SiO<sub>2</sub> mask. InAs wires were grown by molecular beam epitaxy (MBE), with one facet of the triangular cross-section covered with *in-situ* MBE grown Al (Fig. 1a-c). The material growth is described in detail in Ref. [29]. Data from three devices are presented. Device 1 (Fig. 1d) consists of a single barrier at the end of a 4  $\mu$ m wire, defined by a lithographically patterned gate adjacent to a Ti/Au contact where the Al has been removed by wet etching. This device allowed density of states measurement at the end of the

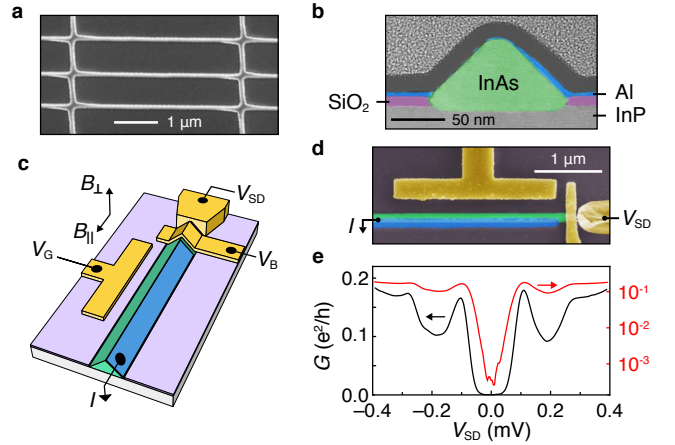


FIG. 1. **Selective area grown hybrid nanowires.** **a**, Scanning electron micrograph of a SAG hybrid network. **b**, False-colored annular dark field scanning transmission electron micrograph of a nanowire cross-section displays InP substrate, InAs (green) nanowire, Al (blue) shell and SiO<sub>2</sub> (purple) mask. **c**, Measurement set-up for device 1 showing the gate voltages and orientations of magnetic fields used in the measurements. **d**, False-colored electron micrograph of device 1. **e**, Differential conductance,  $G$ , as a function of source-drain bias,  $V_{SD}$ , in linear (black) and logarithmic (red) scales shows a hard superconducting gap.

wire by means of bias spectroscopy, to investigate the superconducting proximity effect in the InAs. Evolution of Coulomb blockade in temperature and magnetic field was studied in device 2 (Fig. 2b)—a hybrid quantum dot of length  $1.1\text{ }\mu\text{m}$  defined by two Ti/Au gates adjacent to etched-Al regions. The barrier voltages  $V_B$  were used to create tunneling barriers. The chemical-potential in the wires was tuned with gate voltage  $V_G$ . Device 3 was a micron-size square loop (Fig. 4a) with fully removed Al, which was used to extract phase coherence lengths from weak antilocalization (WAL) and Aharonov-Bohm (AB) oscillations. Standard ac lock-in measurements were carried out in a dilution refrigerator with a three-axis vector magnet. See Methods for more detailed description of the growth, fabrication and measurement setup.

Differential conductance,  $G$ , in the tunneling regime, as a function of source-drain bias,  $V_{SD}$ , for device 1 (Fig. 1e) reveals a gapped density of states with two peaks at  $V_{SD} = 110\text{ }\mu\text{eV}$  and  $280\text{ }\mu\text{eV}$ . We tentatively identify the two peaks with two populations of carriers in the semiconductor, the one with a larger gap residing at the InAs-Al interface and with a smaller at the InAs-InP. The zero-bias conductance is  $\sim 400$  times lower than the above-gap conductance, a ratio exceeding VLS nanowire [11, 23, 30] and 2DEG devices [13], indicating a hard induced gap. We note, however, that co-tunneling through a quantum-dot or multichannel tunneling can enhance this ratio [31].

Transport through a Coulomb island geometry (Fig. 2) at low temperatures shows  $2e$ -periodic peak spacing as a function of  $V_G$ . Coulomb diamonds at finite bias (not shown) yield a charging energy  $E_C = 60\text{ }\mu\text{eV}$ , smaller than the induced gap,  $\Delta^* \sim 100\text{ }\mu\text{eV}$ , as seen in Fig. 1e. The zero-bias Coulomb blockade spacing evolves to even-odd and finally to  $1e$ -periodic peaks with increasing temperature,  $T$ . The  $2e$  to  $1e$  transition in temperature does not result from the destruction of superconductivity, but rather arises due to the thermal excitation of quasiparticles on the island, as investigated previously in metallic islands [32, 33] and semiconductor-superconductor VLS nanowires [34].

A thermodynamic analysis of Coulomb blockade peak spacings is based on the difference in free energies,  $F = F_O - F_E$ , between even and odd occupied states. We consider a simple model that assumes a single induced gap  $\Delta^*$ , not accounting for the double-peaked density of states in Fig. 1e. At low temperatures ( $T \ll E_C, \Delta^*$ ),  $F$  approaches  $\Delta^*$ . Above a characteristic poisoning temperature,  $T_p$ , quasiparticles become thermally activated and  $F$  decreases rapidly to zero. For  $F(T) > E_C$ , Coulomb peaks are  $2e$  periodic with even peak spacings,  $S_E \propto E_C$ , independent of  $T$ . For  $F(T) < E_C$ , odd states become occupied, and the difference in peak spacing,  $S_E - S_O$ , decreases roughly proportional to  $F$ . A full analysis following Ref. [34] (see Methods) yields the peak spacing

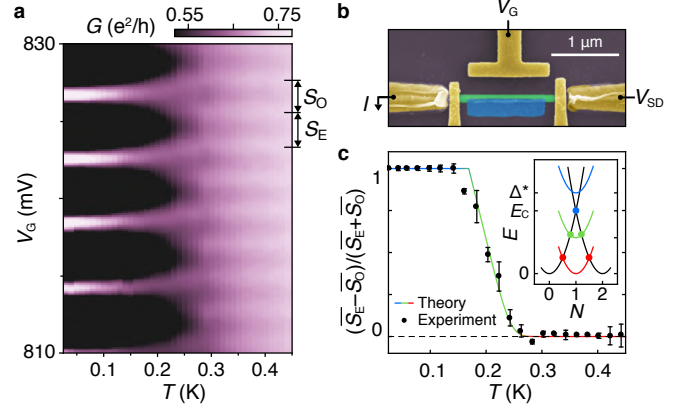


**FIG. 2. Coulomb blockade in temperature.** **a**, Conductance,  $G$ , of device 2 as a function of applied gate voltage,  $V_G$ , and temperature,  $T$ . A characteristic  $2e$  to  $1e$  transition occurs around  $200\text{ mK}$ . The color scale was adjusted for better visibility. **b**, False-colored electron micrograph of device 2. **c**, Normalized even-odd peak spacing difference,  $(\overline{S_E} - \overline{S_O})/(\overline{S_E} + \overline{S_O})$ , from the measurements shown in **b** as a function of  $T$ . The error-bars were estimated using standard deviation of the peak spacing. The theoretical fit corresponds to an induced superconducting gap  $\Delta^* = 190\text{ }\mu\text{eV}$ . Inset: Energy,  $E$ , of the device as a function of normalized gate voltage,  $N$ . Black (colour) parabolas correspond to even(odd)-parity ground state. Transport occurs at the charge degeneracy points indicated by filled circles.

difference

$$\begin{aligned} S_E - S_O &= \frac{2}{\eta e} \min(E_C, F) \\ &= (S_E + S_O) \min(1, F/E_C), \end{aligned} \quad (1)$$

where  $\eta$  is the dimensionless gate lever arm measured from Coulomb diamonds.

Figure 2c shows the measured even-odd difference in peak spacing,  $(\overline{S_E} - \overline{S_O})/(\overline{S_E} + \overline{S_O})$ , averaged over 4 peaks in device 2, along with Eq. (1). Thermodynamic analysis shows an excellent agreement with the peak spacing data across the full range of temperatures. The fit uses an independently measured  $E_C$ , with the induced gap as a single fit parameter, yielding  $\Delta^* = 190\text{ }\mu\text{eV}$ , a reasonable value that lies between the two density of states features in Fig. 1e. The island remains unpoisoned below  $T_p \sim 250\text{ mK}$ .

The evolution of Coulomb blockade peaks with parallel magnetic field,  $B_{\parallel}$ , is shown in Fig. 3a. In this data set, peaks show even-odd periodicity at zero field due to a gate-dependent gap or a bound state at energy  $E_0$  less than  $E_C$ . A subgap state results in even-state spacing proportional to  $E_C + E_0$  and odd-state spacing  $E_C - E_0$  [16] (see Methods), giving

$$\begin{aligned} S_{E,O} &= \frac{1}{\eta e} [E_C \pm \min(E_C, E_0)] \\ &= \frac{S_E + S_O}{2} [1 \pm \min(1, E_0/E_C)]. \end{aligned} \quad (2)$$

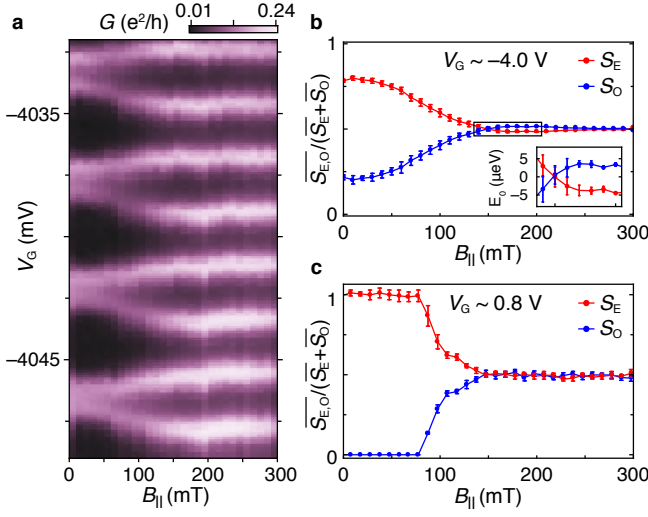


FIG. 3. **Coulomb blockade in magnetic field.** **a**, Conductance as a function of  $V_G$  and  $B_{\parallel}$  from device 2, taken at  $V_G \sim -4.0$  V, shows even-odd peak spacings at zero field transit to  $1e$  spacing when the field is increased. **b**, Normalized even and odd Coulomb peak spacings,  $\overline{S_{E,O}}/(\overline{S_E} + \overline{S_O})$ , from the measurements shown in **a**, as a function of  $B_{\parallel}$ . Inset: zoom-in of the peak spacing overshoot with amplitude of  $7 \mu\text{eV}$  at  $B_{\parallel} = 170$  mT. **c**, Same as **b**, but taken at  $V_G \sim 0.8$  V. At positive gate voltage, the peaks become evenly spaced above  $B_{\parallel} = 150$  mT. The error-bars in **a** and **b** were estimated using the standard deviation of the peak position.

Figure 3b shows the  $B_{\parallel}$  dependence of even and odd peak spacings,  $\overline{S_{E,O}}/(\overline{S_E} + \overline{S_O})$ , extracted from the data in Fig. 3a, giving an effective  $g$ -factor of  $\sim 13$ . Even and odd peak spacings become equal at  $B_{\parallel} = 150$  mT, then overshoot at higher fields with a maximum amplitude corresponding to  $(7 \pm 1) \mu\text{eV}$ . At more positive gate voltages (Fig. 3c), where the carrier density is higher, peaks are  $2e$ -periodic at zero field, then transition through even-odd to  $1e$ -periodic Coulomb blockade without an overshoot, with an effective  $g$ -factor of  $\sim 31$ .

Overshoot of peak spacing, with  $S_O$  exceeding  $S_E$ , indicates a discrete subgap state crossing zero energy [16, 35], consistent with interacting Majorana modes. The overshoot observed at more negative  $V_G$  is quantitatively in agreement with the overshoot seen in VLS wires of comparable length [16]. The absence of the overshoot and the increase of the  $g$ -factor at positive  $V_G$  is consistent with the gate-tunable carrier density in VLS wires [36].

To demonstrate fabrication and operation of a simple SAG network, we investigate the coherence of electron transport in the loop structure shown in Fig. 4a, with the Al layer completely removed by wet etching. Conductance as a function of perpendicular magnetic field,  $B_{\perp}$ , shows a peak around zero magnetic field, characteristic of WAL (Fig. 4b). A fit to a theoretical model for disordered quasi one-dimensional wires with strong spin-orbit coupling [37] yields an electron phase-coherence length

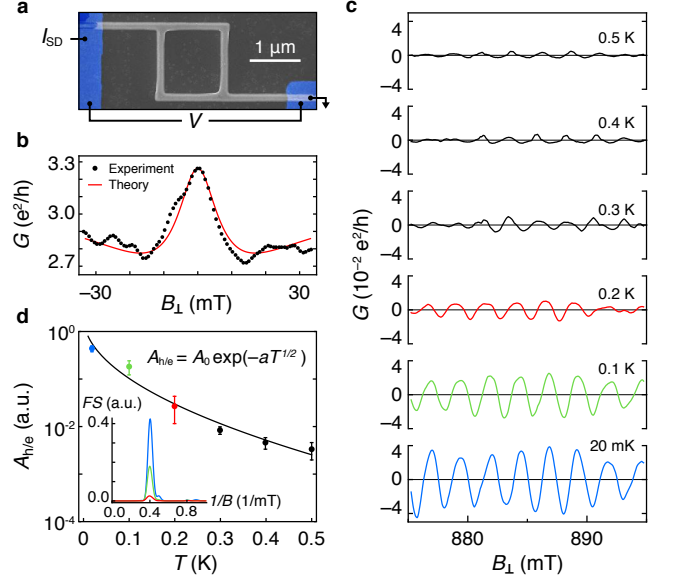


FIG. 4. **Interference effects in a selective area grown loop.** **a**, Electron micrograph of device 3 with false-colored epitaxial Al contacts (blue) and overlaid 4-wire measurement setup. **b**, Conductance,  $G$ , as a function of  $B_{\perp}$ . Red curve is a theoretical magnetoconductance displaying the weak antilocalization effect in a system with spin-orbit length,  $l_{SO} \sim 0.4 \mu\text{m}$ , and phase-coherence length,  $l_{\phi}^{\text{WAL}} \sim 1.2 \mu\text{m}$ . **c**, Aharonov-Bohm oscillations around  $B_{\perp} \sim 900$  mT at different temperatures. **d**, Amplitude of the  $h/e$  oscillations as a function of  $T$ . The exponential fit corresponds to the base-temperature phase-coherence length of  $l_{\phi}^{\text{AB}} = 3.9 \mu\text{m}$ . The error-bars correspond to the standard deviation between 4 data sets. Inset: Fourier spectra,  $FS$ , of the interference signal at 20 mK (blue), 100 mK (green) and 200 mK (red) from the measurements shown in **b**.

$l_{\phi}^{\text{WAL}} \sim 1.2 \mu\text{m}$ , and a spin-orbit length  $l_{SO} \sim 0.4 \mu\text{m}$ .

Upon suppressing WAL with a large perpendicular field periodic conductance oscillations are observed (Fig. 4c) with period  $\Delta B_{\perp} = 2.5$  mT corresponding to  $h/e$  AB oscillations with area  $1.7 \mu\text{m}^2$ , matching the lithographic area of the loop. The oscillation amplitude,  $A_{h/e}$ , measured from the power spectral band around  $h/e$  (Fig. 4d, inset) was observed to decrease with increasing temperature as seen in Fig. 4d. Taking  $A_{h/e} \propto \exp[-L/l_{\phi}^{\text{AB}}(T)]$  with the loop circumference  $L = 5.2 \mu\text{m}$  and  $l_{\phi}^{\text{AB}} \propto T^{-1/2}$  for a diffusive ring [38], a fit of the logarithmic amplitude  $\log(A_{h/e}) = \log(A_0) - aT^{1/2}$  yields  $\log(A_0) \sim 0.7$  and  $a \sim 9 \text{ K}^{-1/2}$  (Fig. 4d), giving a base-temperature phase-coherence length  $l_{\phi}^{\text{AB}}(20 \text{ mK}) \sim 4 \mu\text{m}$ .

The discrepancy between the extracted  $l_{\phi}^{\text{WAL}}$  and  $l_{\phi}^{\text{AB}}$  has previously been observed in an experiment on GaAs/AlGaAs-based arrays of micron-sized loops [39]. It has been argued theoretically that WAL and AB interference processes are governed by different dephasing mechanisms [38]. As a result,  $l_{\phi}^{\text{WAL}}$  and  $l_{\phi}^{\text{AB}}$  have different

temperature dependences.

Our results show that selective area grown hybrid nanowires are an excellent platform for scalable Majorana networks. The hard induced superconducting gap and  $2e$ -periodic Coulomb oscillations imply strongly suppressed quasiparticle poisoning. The overshoot of Coulomb peak spacing in a parallel magnetic field indicates the presence of a discrete low-energy state and is a signature of MZMs. The measured SAG-based network exhibits strong spin-orbit coupling and phase-coherent transport. Furthermore, the ability to design arbitrary hybrid wire networks—a requirement for realizing topological quantum information processing—is readily achievable in SAG. Future work on SAG-based hybrid networks will focus on spectroscopy, correlations, interferometry, and manipulation of MZMs.

## METHODS

### Sample preparation

The InAs nanowires with a triangular cross-sections were selectively grown by MBE along the [100] direction on a semi-insulating (001) InP substrate with a pre-patterned (15 nm) SiO<sub>2</sub> mask [29]. A thin (7 nm) layer of Al was grown *in-situ* at low temperatures on one facet by angled deposition, forming an epitaxial interface with InAs. For the fabrication of the devices, Al was selectively removed using electron-beam lithography and wet etch (Transene Al Etchant D, 50 °C, 10 s). Normal Ti/Al (5/120 nm) ohmic contacts were deposited after *in situ* Ar milling (RF ion source, 15 W, 18 mTorr, 5 min). A film of HfO<sub>2</sub> (7 nm) was applied via atomic layer deposition at 90 °C before depositing Ti/Au (5/100 nm) gate electrodes.

### Measurement setup

The measurements were carried out with a lock-in amplifier at 173 Hz in a dilution refrigerator with a base temperature of 20 mK. For voltage bias measurements, an ac signal with an amplitude of 0.1 V was applied to a sample through a homebuilt resistive voltage-divider (1 : 17.700), resulting in  $V_{AC} \sim 6 \mu\text{V}$  excitation. For current bias, we applied 1 V ac signal to a 1 G $\Omega$  resistor in series with a sample giving  $I_{AC} = 2 \text{ nA}$  excitation.

### Free energy model

The theoretical fit in Fig. 2b is based on a free energy model given in Eq. (1), where the difference in free energy between odd and even occupied states is given by

$$F(T) = k_B T \ln \left[ \frac{(1 + e^{-\Delta^*/k_B T})^{N_{\text{eff}}} + (1 - e^{-\Delta^*/k_B T})^{N_{\text{eff}}}}{(1 + e^{-\Delta^*/k_B T})^{N_{\text{eff}}} - (1 - e^{-\Delta^*/k_B T})^{N_{\text{eff}}}} \right],$$

with the effective number of continuum states  $N_{\text{eff}} = 2V_{\text{Al}}\rho_{\text{Al}}\sqrt{2\Delta^*k_B T}$ , where  $V_{\text{Al}}$  is the volume of the island and  $\rho_{\text{Al}}$  is the density of states at the Fermi energy [32]. The fit was obtained by using  $V_{\text{Al}} = 2.2 \times 10^{-6} \text{ nm}^3$ , consistent with Fig. 2a, electron density of states  $\rho_{\text{Al}} = 23 \text{ eV}^{-1} \text{ nm}^{-3}$  [32] and  $E_C = 60 \text{ meV}$ , measured from Coulomb diamonds, with  $\Delta^*$  as the single fit parameter.

### Device energy

Energy,  $E$ , of a Coulomb blockaded device with electron occupancy,  $n$ , as a function of normalized gate voltage,  $N$ , can be defined as

$$E(N) = E_C(n - N)^2 + FN_0, \quad (3)$$

where  $E_C$  is the charging energy,  $F$  is the relative free energy and  $N_0 = 0$  (1) for even (odd) parity of the device, see Fig. 2c, inset. Charge degeneracy points can be extracted using Eq. (3), from which we can deduce the normalized even and odd peak spacings in units of charge,  $e$ , as

$$N_{\text{E,O}} = 1 \pm F/E_C. \quad (4)$$

The even and odd peak spacing difference in gate voltage is given by

$$S_E - S_O = \frac{E_C}{e\eta}(N_E - N_O), \quad (5)$$

with the dimensionless lever arm  $\eta = E_C/eS$ .

Note that in the limit of zero temperature,  $F$  is defined by the size of the induced gap,  $\Delta^*$ , or, if present, by the energy of a subgap state,  $E_0$ .

## ACKNOWLEDGEMENTS

We thank A. Higginbotham and R. Lutchyn for valuable discussions as well as R. McNeil, C. Sørensen and S. Upadhyay for contributions to material growth and device fabrication. The research was supported by Microsoft Project Q, the Danish National Research Foundation and the European Commission. C.M.M. acknowledges support from the Villum Foundation. M.T.D acknowledges support from State Key Laboratory of High Performance Computing, China. S.M-S. acknowledges funding from "Programa Internacional de Becas "la Caixa"-Severo Ochoa". ICN2 acknowledges support from the Severo Ochoa Programme (MINECO, Grant no. SEV-2013-0295) and is funded by the CERCA Programme / Generalitat de Catalunya. Part of the present work has been performed in the framework of Universitat Autònoma de Barcelona Materials Science PhD program.

# AUTHOR CONTRIBUTIONS

F.K., J.E.S. and P.K. developed the SAG materials. S.V., A.M.W. and L.C. fabricated the devices. S.V. carried out the measurements with input from M.T.D., L.C. and C.M.M. Data analyzing/interpreting and manuscript writing were done by S.V., A.M.W., M.T.D., L.C. and C.M.M. The (S)TEM analyses were performed by S.M.S. and J.A.

- 
- [1] Kitaev, A. Y. Unpaired Majorana fermions in quantum wires. *Physics-Uspekhi* **131**, 130-136 (2001).
  - [2] Read, N. & Green, D. Paired states of fermions in two dimensions with breaking of parity and time-reversal symmetries and the fractional quantum Hall effect. *Phys. Rev. B* **61**, 10267 (2000).
  - [3] Nayak, C., Simon, S. H., Stern, A., Freedman, M. & Das Sarma, S. Non-Abelian anyons and topological quantum computation. *Rev. Mod. Phys.* **80**, 1083-1159 (2008).
  - [4] Das Sarma, S., Freedman, M. & Nayak, C. Majorana Zero Modes and Topological Quantum Computation. *NJP Quantum Information* **1**, 15001 (2015).
  - [5] Alicea, J., Oreg, Y., Refael, G., von Oppen, F. & Fisher, M. P. A. Non-Abelian statistics and topological quantum information processing in 1D wire networks. *Nat. Phys.* **7**, 412-417 (2011).
  - [6] Aasen, D. *et al.* Milestones Toward Majorana-Based Quantum Computing. *Phys. Rev. X* **6**, 031016 (2016).
  - [7] Flensberg, K. Non-Abelian Operations on Majorana Fermions via Single-Charge Control. *Phys. Rev. Lett.* **106**, 090503 (2011).
  - [8] Plugge, S., Rasmussen, A., Egger, R. & Flensberg, K. Majorana box qubits. *New J. Phys.* **19**, 012001 (2017).
  - [9] Vijay, S & Fu, L. Teleportation-based quantum information processing with Majorana zero modes. *Phys. Rev. B* **94**, 235446 (2016).
  - [10] Karzig, T. *et al.* Scalable designs for quasiparticle-poisoning-protected topological quantum computation with Majorana zero modes. *Phys. Rev. B* **95**, 235305 (2017).
  - [11] Gazibegovic, S. *et al.* Epitaxy of advanced nanowire quantum devices. *Nature* **548**, 434-438 (2017).
  - [12] Shabani, J. *et al.* Two-dimensional epitaxial superconductor-semiconductor heterostructures: A platform for topological superconducting networks. *Phys. Rev. B* **93**, 155402 (2016).
  - [13] Kjaergaard, M. *et al.* Quantized conductance doubling and hard gap in a two-dimensional semiconductor-superconductor heterostructure. *Nat. Commun.* **7**, 12841 (2016).
  - [14] Suominen, H. J. *et al.* Zero-Energy Modes from Coalescing Andreev States in a Two-Dimensional Semiconductor-Superconductor Hybrid Platform. *Phys. Rev. Lett.* **119**, 176805 (2017).
  - [15] Nichele, F. *et al.* Scaling of Majorana Zero-Bias Conductance Peaks. *Phys. Rev. Lett.* **119**, 136803 (2017).
  - [16] Albrecht, S. M. *et al.* Exponential Protection of Zero Modes in Majorana Islands. *Nature* **531**, 7593 (2016).
  - [17] Lutchyn, R., Sau, J. D. & Das Sarma, S. Majorana Fermions and a Topological Phase Transition in semiconductor-superconductor Heterostructures. *Phys. Rev. Lett.* **105**, 077001 (2010).
  - [18] Oreg, Y., Refael, G. & von Oppen, F. Helical Liquids and Majorana Bound States in Quantum Wires. *Phys. Rev. Lett.* **105**, 177002 (2010).
  - [19] Krogstrup, P. *et al.* Epitaxy of semiconductor-superconductor nanowires. *Nat. Mat.* **14**, 400-406 (2015).
  - [20] Mourik, V. *et al.* Signatures of Majorana Fermions in Hybrid Superconductor-Semiconductor Nanowire Devices. *Science* **336**, 1003-1007 (2012).
  - [21] Deng, M. T. *et al.* Anomalous Zero-Bias Conductance Peak in a Nb-InSb Nanowire-Nb Hybrid Device. *Nano Lett.* **12**, 6414-6419 (2012).
  - [22] Das, A. *et al.* Zero-bias peaks and splitting in an Al-InAs nanowire topological superconductor as a signature of Majorana fermions. *Nat. Phys.* **8**, 887-895 (2012).
  - [23] Zhang, H. *et al.* Ballistic Majorana nanowire devices, *arXiv:1603.04069* (2016).
  - [24] Deng, M. T. *et al.* Majorana bound state in a coupled quantum-dot hybrid-nanowire system. *Science*, **354**, 6319 (2016).
  - [25] Zhang, H., *et al.* Quantized Majorana conductance. *arXiv:1710.10701* (2017).
  - [26] Sestoft, J. E. *et al.* Engineering Hybrid Epitaxial InAsSb/Al Nanowire Materials for Stronger Topological Protection. *arXiv:1711.06864* (2017).
  - [27] Sherman, D. *et al.* Normal, superconducting and topological regimes of hybrid double quantum dots. *Nat. Nanotechnol.*, 212-217 (2017).
  - [28] Krizek, F. *et al.* Growth of InAs Wurtzite Nanocrosses from Hexagonal and Cubic Basis. *Nano Lett.* **17**, 6090-6096 (2017).
  - [29] Krizek, F. *et al.* Scalable quantum nanowire networks grown by molecular beam epitaxy. *submitted* (2018).
  - [30] Chang, W. *et al.* Hard gap in epitaxial semiconductor-superconductor nanowires. *Nat. Nanotechnol.* **10**, 232-236 (2015).
  - [31] Beenakker, C. W. J. Quantum transport in semiconductor-superconductor microjunctions. *Phys. Rev. B* **46**, 12841-12844 (1992).
  - [32] Tuominen, M. T., Hergenrother J. M., Tighe T. S., & M. Tinkham, M. Experimental evidence for parity-based 2e periodicity in a superconducting single-electron tunneling transistor. *Phys. Rev. Lett.* **69**, 1997 (1992).
  - [33] Lafarge, P., Joyez, P., Esteve, D., Urbina, C. & Devoret, M. H. Measurement of the even-odd free-energy difference of an isolated superconductor. *Phys. Rev. Lett.* **70**, 994-997 (1993).
  - [34] Higginbotham, A. P. *et al.* Parity lifetime of bound states in a proximitized semiconductor nanowire. *Nat. Phys.* **11**, 1017-1021 (2015).
  - [35] Chiu, C.-K., Sau J. D., & Das Sarma, S. Conductance of a superconducting Coulomb-blockaded Majorana nanowire. *Phys. Rev. B* **96**, 054504 (2017).
  - [36] Vaitiekėnas, S., Deng, M. T., Nygård, J., Krogstrup, P. & Marcus, C. M. Effective  $g$ -factor in Majorana Wires. *arXiv:1710.04300* (2017).
  - [37] Kurdak, C., Chang, A., Chin, A. & Chang, T., Quantum interference effects and spin-orbit interaction in quasi-one-dimensional wires and rings. *Phys. Rev. B* **46**, 6846 (1992).

- [38] Ludwig, T. & Mirlin, A. D. Interaction-induced dephasing of Aharonov-Bohm oscillations T. *Phys. Rev. B.* **69**, 193306 (2004).
- [39] Ferrier, M. *et al.* Geometrical Dependence of Decoherence by Electronic Interactions in a GaAs/GaAlAs Square Network. *Phys. Rev. Lett.* **100**, 146802 (2008).